Materials Horizons

ROYAL SOCIETY OF CHEMISTRY

COMMUNICATION

View Article Online
View Journal

Cite this: DOI: 10.1039/d6mh00390g

Received 2nd March 2026,
Accepted 20th April 2026

DOI: 10.1039/d6mh00390g

rsc.li/materials-horizons

Programmable ion–protein networks from sodium caseinate: a sustainable platform for soft functional materials

Pietro Tordi, [ab] Verónica Montes-García, [ac] Virginia Losasso,[b] Artur Ciesielski, [ac] Paolo Samorì *[a] and Massimo Bonini *[b]

Ion–protein coordination represents an underexploited design principle to assemble multiresponsive, soft, sustainable materials. Here, we harness sodium caseinate to construct programmable ionically crosslinked hydrogels in which multivalent cation selection governs the network architecture and enables a broad tunability of mechanical and other functional properties. A systematic study of cation types, including Ca^{2+}, Sr^{2+}, Ba^{2+}, Mn^{2+}, Cu^{2+}, Zn^{2+}, Fe^{3+}, Al^{3+}, and Zr^{4+}, revealed pronounced ion-specific control over mechanical stiffness (1.5 kPa to 1.8 MPa), thermal stability, and hierarchical architecture. Multimodal characterization of their compositional, structural, morphological, thermal, spectroscopic, and mechanical properties enabled the tailoring of an empirical packing hierarchy for M^{X+}-caseinate networks (MCas). Leveraging this tunability, we demonstrate proof-of-concept piezoresistive soft sensors in which ionic crosslinking of caseinate modulates the mechanical properties of caseinate–gelatin organohydrogel matrices. These matrices, crosslinked with Sr^{2+} and Zn^{2+}, exhibit linear $\Delta R/R_0$ responses with gauge factors (1.84–2.20) competitive with state-of-the-art organohydrogel sensors. Real-time measurements further demonstrate their ability to detect bending angles and encode dynamic inputs, such as Morse code signals. These results position MCas as a sustainable, ion-tunable platform for the rational design of mechanically programmable protein hydrogels, opening opportunities in bioinspired materials for soft electronics and wearable sensing.

New concepts

This work reframes ion–protein coordination from a local crosslinking motif into a programmable design principle for soft multifunctional materials. We show that a widely available, low-cost protein (sodium caseinate) can be converted into a family of mechanically and structurally tunable hydrogels by changing only the identity of the coordinating multivalent ions, without altering polymer chemistry or introducing covalent crosslinks. In contrast to most ionic gels, which are dominated by polysaccharide systems or isolated, case-specific chemistries, we establish protein-based ionic networks as a distinct and general materials class. Crucially, we introduce an operational packing hierarchy that links ion coordination to nanoscale organization and macroscopic function within a unified framework. The central conceptual advance is that ion identity itself becomes an independent "programming variable", enabling rational control of network density, stiffness, and electromechanical response across orders of magnitude. This work provides a transferable strategy for designing protein-based ionic soft matter, bridging molecular coordination, multiscale structure, and emergent function, opening a new route to sustainable, mechanically programmable materials for soft electronics and beyond.

Introduction

Soft electronics use compliant, water-rich materials that convert mechanical inputs into electrical signals without sacrificing biocompatibility and mechanical conformity.[1] Hydrogels, with their extreme stretchability, fast ion transport, and tissue-like softness, have become key components in soft electronics, powering advances in wearable sensors, biointerfaces, and soft robotics.[1] Within this evolving landscape, biopolymer-based hydrogels are rapidly gaining attention. Their intrinsic sustainability, structural diversity and chemical functionality offer advantages over synthetic counterparts, particularly for systems where environmental compatibility or biological interfacing is crucial.[1–4] In addition, the increasing demand for greener technologies has intensified the search for low-cost, renewable biopolymers that can provide both mechanical robustness and tunable functional responses.[2,5]

Unfortunately, the translation of biopolymers into functional materials remains nontrivial. Many natural polymers exhibit inherent batch-to-batch variability, limited structural uniformity, and insufficient mechanical resilience under cyclic deformation. Moreover, their complex molecular architectures often limit the independent tuning of their properties,

[a] University of Strasbourg & CNRS, ISIS & icFRC, 8 Allée Gaspard Monge, 67000 Strasbourg, France. E-mail: samori@unistra.fr
[b] University of Florence, DICUS, via della Lastruccia 3, Sesto Fiorentino, 50019, Italy. E-mail: massimo.bonini@unifi.it
[c] Center for Advanced Technologies, Adam Mickiewicz University, Uniwersytetu Poznańskiego 10, Poznań 61-614, Poland

jeopardizing their optimization and long-term reliability. These constraints underscore the need for identifying biopolymers capable of forming mechanically programmable networks *via* simple fabrication strategies while retaining strong potential for functional property tuning. In this context, alginate, a widely studied polyanionic polysaccharide, has recently emerged as a prototypical system. Alginate forms stable and robust ionic hydrogels with divalent or trivalent cations and has been broadly applied in biomedical and energy contexts, as the ions act not only as a source of specific functionality, but also as structuring agents.[6–9] However, alginate lacks the chemical complexity and tunable secondary structure of proteins.[10,11] Proteins represent unique, versatile platforms for advanced materials design, as their amino acid sequences encode a rich array of functional groups that dictate conformational flexibility and multivalent interaction motifs.[12–16] Their intrinsic conformational adaptability and rich repertoire of reversible non-covalent interactions further expand their self-assembly behavior, making proteins attractive building blocks for smart hydrogels whose network properties can be modulated by external stimuli.[17] These features rule the process of self-assembly, yielding a broadest variety of supramolecular architectures, including liquids, gels, fibers, and crystalline lattices. Despite these potentials, widely available natural proteins from industrial byproducts are still rarely explored in material design. Sodium caseinate, a milk-derived protein abundant in dairy byproducts, offers an amphiphilic, polyelectrolytic matrix rich in carboxylate and amine groups capable of coordinating multivalent cations and forming supramolecular networks.[18–22] The coordination behavior of these functional groups depends on ion charge density and coordination environment, determining whether ion binding promotes network formation or protein collapse and precipitation in dilute systems. Its amphiphilic character and chemical versatility make caseinate an attractive candidate for sustainable materials design. However, strategies for structuring it into robust, water-insoluble materials remain limited.

To date, the structuring of caseinate has primarily relied on enzymatic crosslinking *via* transglutaminase,[23,24] or on ionic complexation under dilute conditions.[25–27] While the latter approach has provided insights into protein–ion interactions, it has not been used to produce physically crosslinked hydrogels with sufficient mechanical integrity or practical utility. Consequently, caseinate remains largely absent from the rapidly expanding field of ionic gels for functional materials.[6,28–33] The present work builds on the hypothesis that concentrated sodium caseinate (NaCas), despite its micellar nature and relatively low molecular weight, could form cohesive hydrogels with useful functional performance *via* direct coordination with multivalent cations, provided sufficient proximity between chains is achieved. This approach would enable the generation of programmable protein networks governed by ion identity. Such control could allow precise modulation of hybrid system functions with potential applications in fields such as tissue engineering, bioelectronics, soft robotics, and energy storage.

Here, we report the self-assembly-mediated synthesis of ionically crosslinked caseinate hydrogels (MCas) using a broad library of multivalent cations (Ca^{2+}, Sr^{2+}, Ba^{2+}, Mn^{2+}, Cu^{2+}, Zn^{2+}, Fe^{3+}, Al^{3+}, Zr^{4+}). This ion library was selected to systematically probe the role of cation valency, size, coordination geometry, and associated pH conditions on protein assembly. We demonstrate that cation-caseinate interaction drives network formation and directly governs structural hierarchy and macroscopic properties. Small-angle X-ray scattering (SAXS) reveals cation-dependent differences in the average spacing between crosslinked domains, quantified as correlation lengths ranging from 6.4 nm (loose networks) to 1.0 nm (densely packed). These nanoscale features strongly correlate with the observed porosity and mechanical properties (compressive modulus: 1.5 kPa to 1.8 MPa) of the hydrogels.

As a proof-of-concept application, we selected two representative MCas systems for device integration: ZnCas, embodying the stiffest and most compact network, and SrCas, representing the softer and more compliant one. These hydrogels were combined with gelatin and glycerol into hybrid organohydrogels (MGelCas), where the ionic crosslinking of caseinate provides a direct and powerful handle to program tensile stiffness, extensibility, and network packing. More broadly, this hybrid strategy also provides a practical route to mitigate the brittleness of densely crosslinked caseinate networks while preserving their mechanical reinforcement. Such ion-dependent mechanical tunability is particularly attractive for soft-electronics applications, where strain sensitivity and deformation-dependent transport emerge from the interplay between network density and ionic mobility. Leveraging this tunability, we show that caseinate-based organohydrogels can function as piezoresistive soft sensors, translating mechanical deformation into reproducible electrical signals. By transforming a widely available dairy-industry byproduct into a tunable, ion-responsive functional matrix, M^{X+}-caseinate crosslinking expands the design space of protein-based materials and introduces a previously unexplored route to sustainable, mechanically programmable soft electronics.

Results and discussion

Ion-driven assembly of caseinate hydrogels

Concentrated sodium caseinate (20% w/v) undergoes rapid gelation upon exposure to multivalent cations, yielding robust, shape-stable hydrogels. The addition of a 0.5 M aqueous solution of the corresponding metal chloride (MCl_X) to NaCas leads to the immediate formation of cohesive, free-standing networks. Despite the conceptual simplicity of this approach (Section S1.2, SI), such materials have remained underexplored and mostly limited to food structuring and delivery of bioactives[34]—likely because caseinate's relatively low molecular weight and micelle-like aggregation in dilute media obscure its latent ability to form ion-bridged networks. In contrast to prior work on dilute dispersions or enzymatic covalent routes, we show that concentrated NaCas yields stable, percolated ionic networks by simple coordination, provided chain proximity is ensured. In the specific case of Fe^{3+}, Al^{3+}, and Zr^{4+}, their salt solutions are strongly acidic (pH < 3); under these conditions, partial protonation of caseinate could accompany metal-ion coordination (Section S1.2, SI). Fig. 1a illustrates the

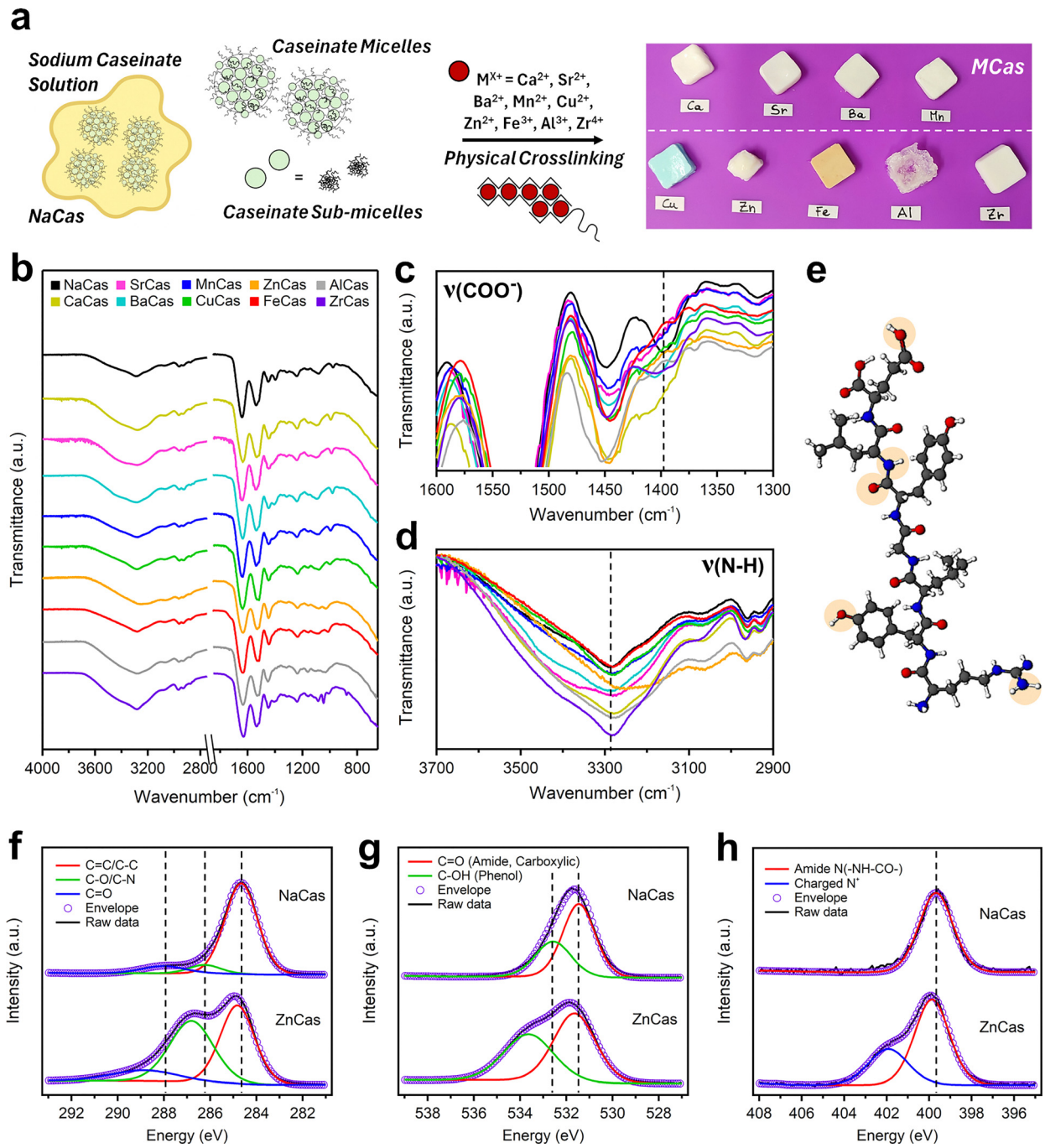

Fig. 1 (a) Schematic of NaCas micelle formation in solution (left) and ionic crosslinking with multivalent metal ions (M^{X+} = Ca^{2+}, Sr^{2+}, Ba^{2+}, Mn^{2+}, Cu^{2+}, Zn^{2+}, Fe^{3+}, Al^{3+}, Zr^{4+}), forming metal-caseinate (MCas) hydrogels with distinct appearances (right). (b) FTIR spectra of NaCas and MCas samples showing metal-dependent shifts. Enlarged regions highlighting changes in (c) carboxylate asymmetric stretching and (d) N–H stretching, indicating coordination with carboxyl and amino groups. (e) Casein peptide model in which residues involved in metal binding are highlighted. High-resolution XPS spectra of NaCas and ZnCas: (f) C 1s, (g) O 1s, (h) N 1s. FTIR spectra are offset for clarity; the assignments of the most significant bands are reported in Table S2. FTIR and XPS spectra are normalized with respect to the most intense peak.

crosslinking mechanism producing MCas hydrogels (M = Ca, Sr, Ba, Mn, Cu, Zn, Fe, Al, Zr) and photographs of the resulting samples, prepared in molds and portrayed after removal.

Distinct ion-polymer coordination behaviors translate into macroscopic differences in texture and appearance. ZnCas and AlCas show pronounced volumetric contraction during gelation (Table S1), consistent with higher effective crosslink density and coordination-induced dehydration. Conversely, alkaline-earth-crosslinked gels (Ca/Sr/Ba) appear softer and more elastic, indicating weaker effective coordination.

Inductively coupled plasma atomic emission spectroscopy (ICP-AES) (Table S1) shows that the ion retention spans from

around 0.4 to 1.5 millimoles per gram of caseinate. These differences reflect a multivariate interplay of ionic radius, charge density, hydration energy, and specific affinity for caseinate functional groups, providing a tunable handle to modulate network architecture and properties.

Fourier-transform infrared spectroscopy (Fig. 1b) unveils the coordinating motifs. Across all MCas samples, the symmetric carboxylate stretching [$\nu_{sym}(COO^-)$] near 1398 cm^{-1} shifts to higher wavenumbers (Fig. 1c and Table S2), highlighting carboxylate participation in coordination. For CuCas, ZnCas, FeCas, and AlCas, this band shifts enough to overlap with the δN–H mode (near 1446 cm^{-1}), preventing separate resolution of the two features. In addition, all MCas samples show perturbations in the N-H stretching region ($\sim$3280 cm^{-1}; Fig. 1d and Table S2). In Zn^{2+}-crosslinked gels, a pronounced downshift (3291 $\rightarrow$ 3252 cm^{-1}) points to stronger interactions of nitrogen-containing groups and/or reinforced hydrogen bonding within the coordinated network—coherent with the tight network formation and volumetric contraction observed for ZnCas.

To further probe the coordination environment, X-ray photoelectron spectroscopy (XPS) is performed on all MCas samples (representative spectra for NaCas and ZnCas in Fig. 1f–h; full datasets in Fig. S1–S9). In ZnCas, the C 1s region (Fig. 1f) shows increased intensity and broadening of both the C=O and C–O/C–N components, consistent with coordination to carboxylate, amide oxygen, and amine-linked carbon atoms. The O 1s region (Fig. 1g) exhibits analogous broadening of the carbonyl contribution. In the N 1s region (Fig. 1h), a higher-binding-energy N^+ component ($\sim$402 eV) emerges alongside a slight upshift of the amide-N peak, indicating partial involvement of nitrogen sites and the appearance of positively polarized/protonated nitrogen. The other MCas systems display similar spectral signatures, emerging as component broadening, noticeable chemical-shift, and N^+ varying in intensity. CaCas deviates only in the latter, highlighting calcium preferential interaction with C=O and C–O moieties. These XPS results fully align with FTIR findings, confirming that multivalent cations interact with both carboxylate and amide/amine functionalities.

Ion-dependent segmental dynamics and nanoscale packing

To directly correlate ionic coordination to macroscopic function, we probe the segmental dynamics of the networks by differential scanning calorimetry (DSC). (Fig. 2a). Glass-transition temperature (T_g) is a sensitive gauge of chain mobility and network rigidity, and therefore crucial to understanding how ion identity governs the structural and mechanical response of MCas hydrogels. As summarized in Fig. 2c and Table S3, gels crosslinked with alkaline-earth ions (Ca^{2+}, Sr^{2+}, Ba^{2+}) exhibit glass-transition temperatures comparable to native NaCas ($\sim$72.2 °C), indicating only minor restrictions of chain mobility. In contrast, interactions with transition metal and high-valent ions (Mn^{2+}, Cu^{2+}, Zn^{2+}, Fe^{3+}, Al^{3+}, Zr^{4+}) shift T_g upward—up to 76.6 °C for AlCas—consistent with tighter interchain coordination and suppressed segmental dynamics.[8,35,36]

While DSC provides crucial information on segmental dynamics, SAXS allows to gain a deeper structural insight by resolving how ion identity dictates nanoscale packing within the hydrated networks. (Fig. 2b and Section S6, SI). Dispersions of NaCas display a broad peak at $q \approx 0.031$ $Å^{-1}$ ($d = 2\pi/q$ = 20.3 nm), indicative of a weak structure-factor arising from short-range correlations (*i.e.*, center-to-center distance) among micelle-like caseinate aggregates. Upon ionic crosslinking, this correlation peak disappears, and the profiles are well described by a Porod–Lorentzian model (eqn (S2)), consistent with a percolated, disordered polymer network lacking inter-aggregate order (Fig. 2e). For cross-sample comparison, we refer to the primary correlation length (ξ_1), *i.e.*, the dominant low-q Lorentzian term, corresponding to the average spacing between crosslinked domains (Fig. 2d).[8,35,37–40] In a subset of samples, an additional high-q feature (ξ_2) was found, which reflects a shorter-range substructure but does not alter the ξ_1-based ranking (Table S4). Based on ξ_1, BaCas, SrCas, MnCas, and CaCas exhibit long values (4.7–6.4 nm), indicating relatively loosely-packed structures. CuCas, FeCas, AlCas, and ZrCas show intermediate densities ($\xi_1 \approx$ 2.3–2.9 nm), while ZnCas stands out with the shortest ξ_1 (1.0 nm), consistent with its ultracompact nanoarchitecture and marked volumetric shrinkage at the macroscale. Importantly, this ξ_1-based structural hierarchy mirrors the mechanical stiffness trends shown below, indicating that ion identity governs nanoscale packing and compaction. Together, the DSC and SAXS results establish that cation identity dictates network packing, which hierarchically propagates to govern macroscopic properties, ranging from structural rigidity to electrochemical performance.

From nanoscale packing to microscale architecture

Having established the nanoscale packing hierarchy of MCas hydrogels, we next investigate how internal organization governs the microscale architecture of the dried materials. Scanning electron microscopy (SEM) of freeze-dried gels reveals marked differences in porosity and structural texture that directly reflect the identity of the coordinating ion (Fig. 3). Notably, variations in ξ_1 report on ion-dependent nanoscale density fluctuations within the hydrated network, whereas the similar morphologies observed by SEM arise from the mesoscale topology of the dried skeleton and therefore do not mirror these local structural differences.[41,42]

Hydrogels crosslinked with the alkaline-earth Ca^{2+}, Sr^{2+}, and Ba^{2+} form highly porous, interconnected networks with well-defined macropores (Fig. 3b, c and Fig. S11–S13). MnCas displays a similar morphology, suggesting that despite its distinct chemical nature, Mn^{2+} enables a comparably open network (Fig. S14), likely due to its lower charge density and weaker coordination affinity.

In contrast, ZnCas, FeCas, and ZrCas yield compact, finely textured architectures with small porosities and high uniformity (Fig. 3d, e and Fig. S16, S17, S19), indicative of densely coordinated polymer networks. AlCas also forms a compact network, but with irregular features—alternating domains of pronounced porosity and nearly pore-free regions (Fig. S18). This heterogeneous pattern suggests uneven local crosslinking and phase separation during gelation. CuCas instead exhibits an intermediate morphology, combining characteristics of both regimes (Fig. S15). This structure aligns with a moderate coordination affinity and crosslinking density.

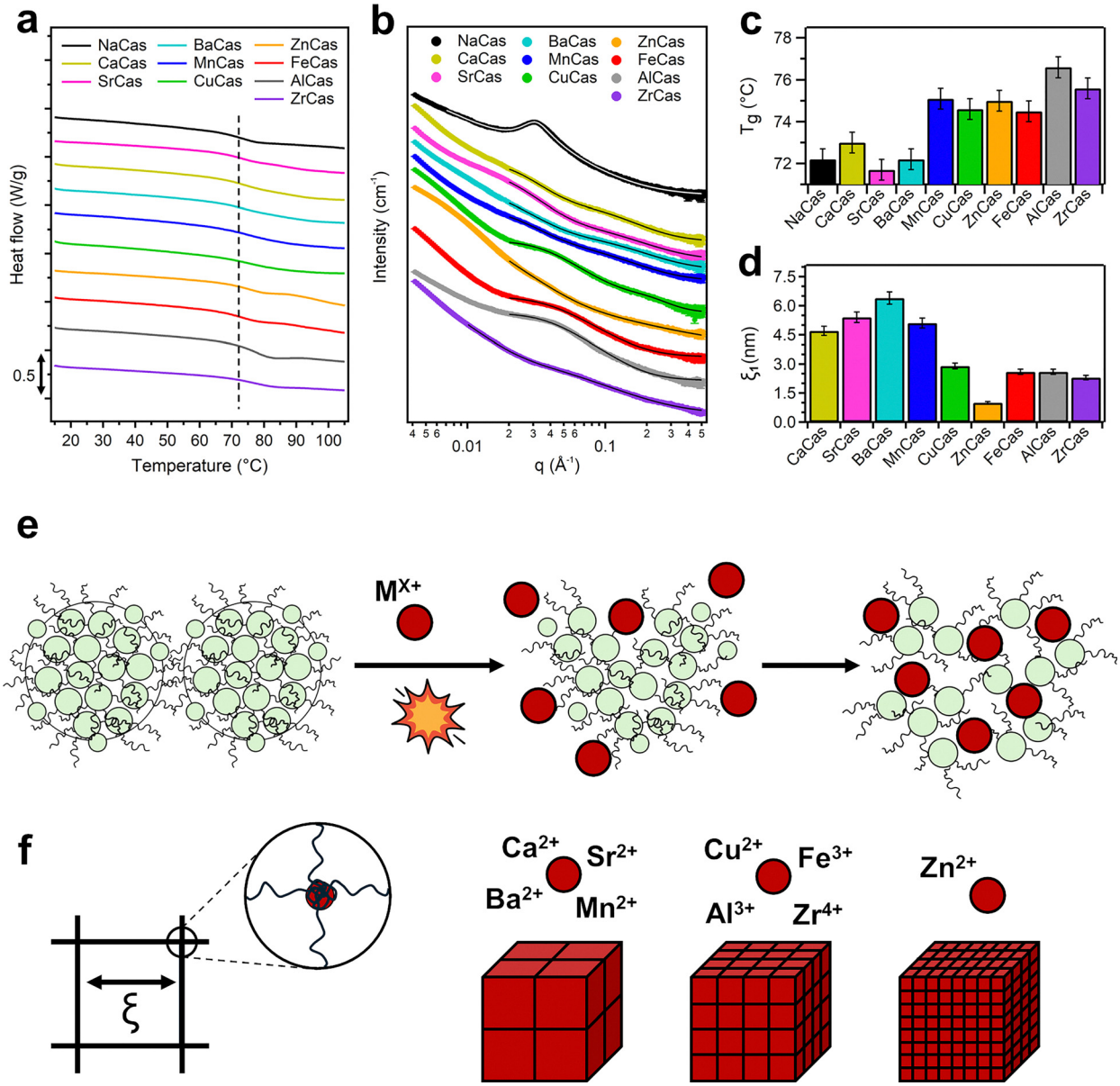

Fig. 2 (a) DSC thermograms and (b) SAXS curves of NaCas and MCas gels. The fitting curves are shown as continuous black lines, except for NaCas, whose fit is shown in white. (c) Extracted T_g values and (d) correlation lengths (ξ) for NaCas and MCas, highlighting how ionic crosslinking governs polymer chain assembly. (e) Schematic illustration of the transition from micellar dispersions to ionically crosslinked networks *via* M^{X+} coordination. (f) Conceptual visualization of the influence of cation identity on nanostructural packing and correlation length.

These observations confirm that the coordinating ion governs not only nanoscale packing but also emergent microscale architecture. The ability to modulate porosity and morphological density through ionic crosslinking offers a versatile, bio-inspired route to tailor material properties across hierarchical length scales. We demonstrate that this morphological hierarchy directly governs bulk properties, including mechanical stiffness and, potentially, solvent transport.

Mechanical performance and operational packing hierarchy

Compressive testing (Fig. 4 and Fig. S20, Table S5) underscores how crosslinking cations rule the mechanical performance of MCas hydrogels, yielding networks that vary widely in stiffness—with compressive moduli spanning over two orders of magnitude across the series. ZnCas exhibits the highest stiffness (1.8 MPa), followed by FeCas (844 kPa), AlCas (557 kPa), and ZrCas (359 kPa). These values are in excellent agreement with the densest nanostructures and most compact morphologies observed *via* SAXS and SEM. In contrast, CaCas, SrCas, BaCas, and MnCas form the softest gels (CM $\leq$ 11.4 kPa), consistent with their loosely packed networks and open porosity. CuCas occupies an intermediate regime (76 kPa), further supporting its transitional coordination behavior.

These results establish a direct correlation between ionic interaction strength, nanoscale packing, and bulk mechanical response. Ion identity serves as a powerful design lever to tune

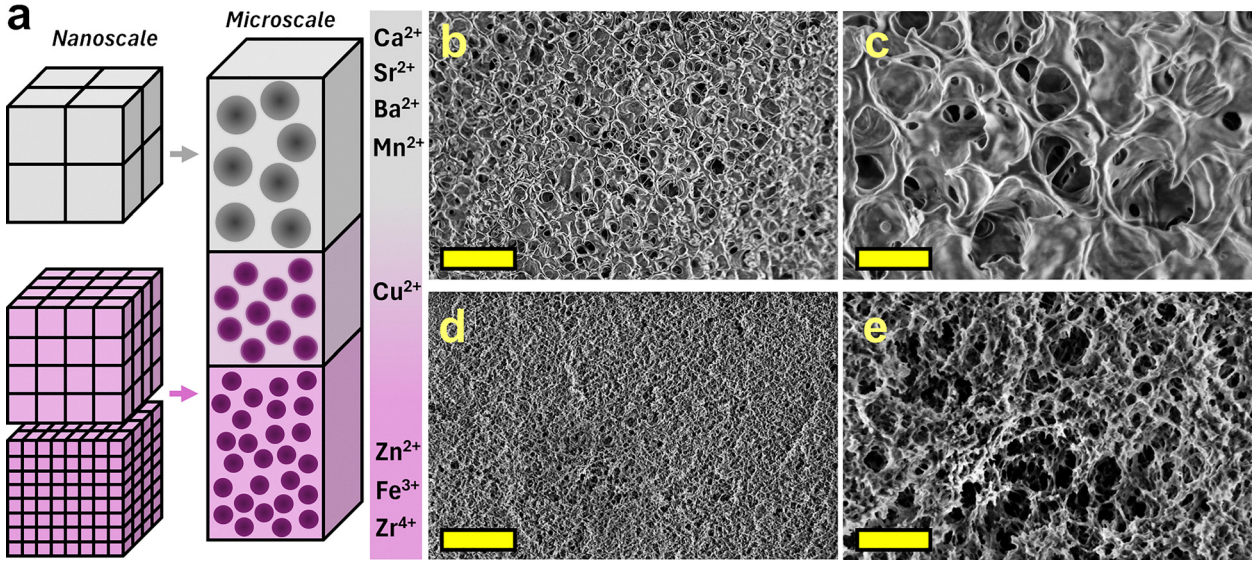

Fig. 3 (a) Schematic representation of the relationship between nanoscale packing density (left) and resulting microscale porosity (right), as modulated by cation identity. Loosely packed nanonetworks (*e.g.* Ca^{2+}, Sr^{2+}, Ba^{2+}, Mn^{2+}) give rise to large, well-defined pores, whereas densely crosslinked systems (*e.g.* Zn^{2+}, Fe^{3+}, Zr^{4+}) form compact architectures with minimal porosity. AlCas is not included, due to its irregular morphology. (b) and (c) SEM images of freeze-dried CaCas hydrogels, representative of SrCas, BaCas, and MnCas. (d) and (e) SEM images of freeze-dried ZnCas hydrogels, representative of FeCas, and ZrCas. Scale bars: 8 μm (b) and (d); 2 μm (c) and (e).

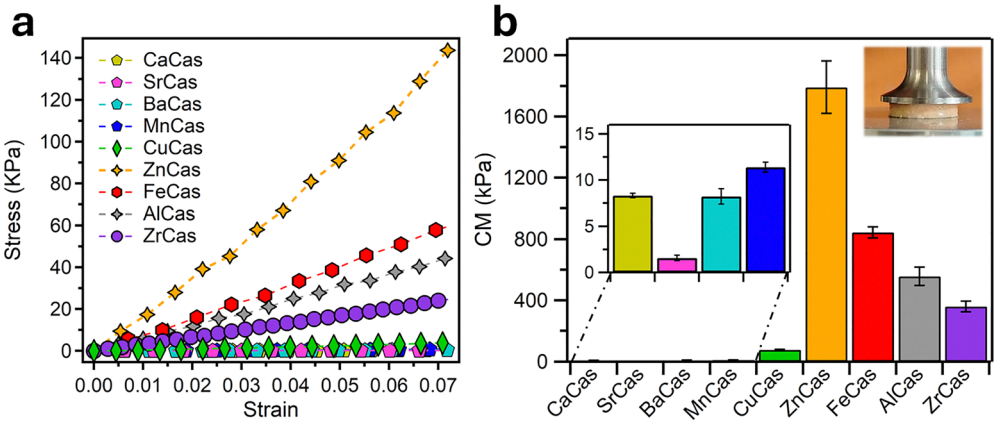

Fig. 4 (a) Compressive stress–strain curves showing cation-dependent stiffness; Full range curves in Fig. S20. (b) Compressive modulus (CM) values, with ZnCas as the stiffest and CaCas, SrCas, BaCas and MnCas as the softest. CuCas shows intermediate stiffness. Inset: expanded view of the soft MCas hydrogels' CM values.

mechanical performance without altering the protein backbone—enabling application-specific tailoring.

Upon integrating DSC, SAXS, SEM, and compressive mechanics, we define an operational packing hierarchy for MCas hydrogels (20% w/v NaCas; 0.5 M MCl_X; hydrated): $Zn^{2+} > Fe^{3+} \sim Al^{3+} \sim Zr^{4+} > Cu^{2+} > Mn^{2+} > Ca^{2+} \sim Sr^{2+} \sim Ba^{2+}$. The ranking combines systematic T_g shifts (DSC), progressive shortening of ξ_1 (SAXS), microstructural densification (SEM), and rising CM (mechanical testing), and captures network compaction rather than intrinsic binding affinity. Crucially, this multi-technique hierarchy establishes a practical design rule for selecting ions to dial stiffness and porosity—providing a generalizable guideline for tailoring protein-based hydrogels.

Taken together, these results position MCas hydrogels as versatile platforms for applications requiring mechanically robust, water-rich, and ion-retentive matrices—spanning tissue engineering, drug delivery, and environmental remediation. Beyond this generic functionality, ion identity serves as an additional design lever: Cu^{2+} can impart antimicrobial activity, while Fe^{3+} and Zn^{2+} may introduce redox or catalytic functionality, further broadening the application landscape. Consistently, MCas hydrogels retain mobile ions that form percolated aqueous pathways, yielding measurable ion-dependent ionic conductivity even after extensive washing (Table S6), underscoring the sustained ion retention and mobility within the protein network.

From ion-controlled mechanics to piezoresistive soft sensors

Building on this multi-technique structural and mechanical hierarchy, we next examined how ion-directed network compaction translates into piezoresistive performance, a key functional response in soft-material sensing. While MCas hydrogels inherently retain mobile counterions (Table S6), enabling moderate ionic conductivity, their distinct mechanical regimes suggest that strain-dependent perturbations of percolated aqueous pathways could be harnessed to realize wearable biopolymer-based sensors.

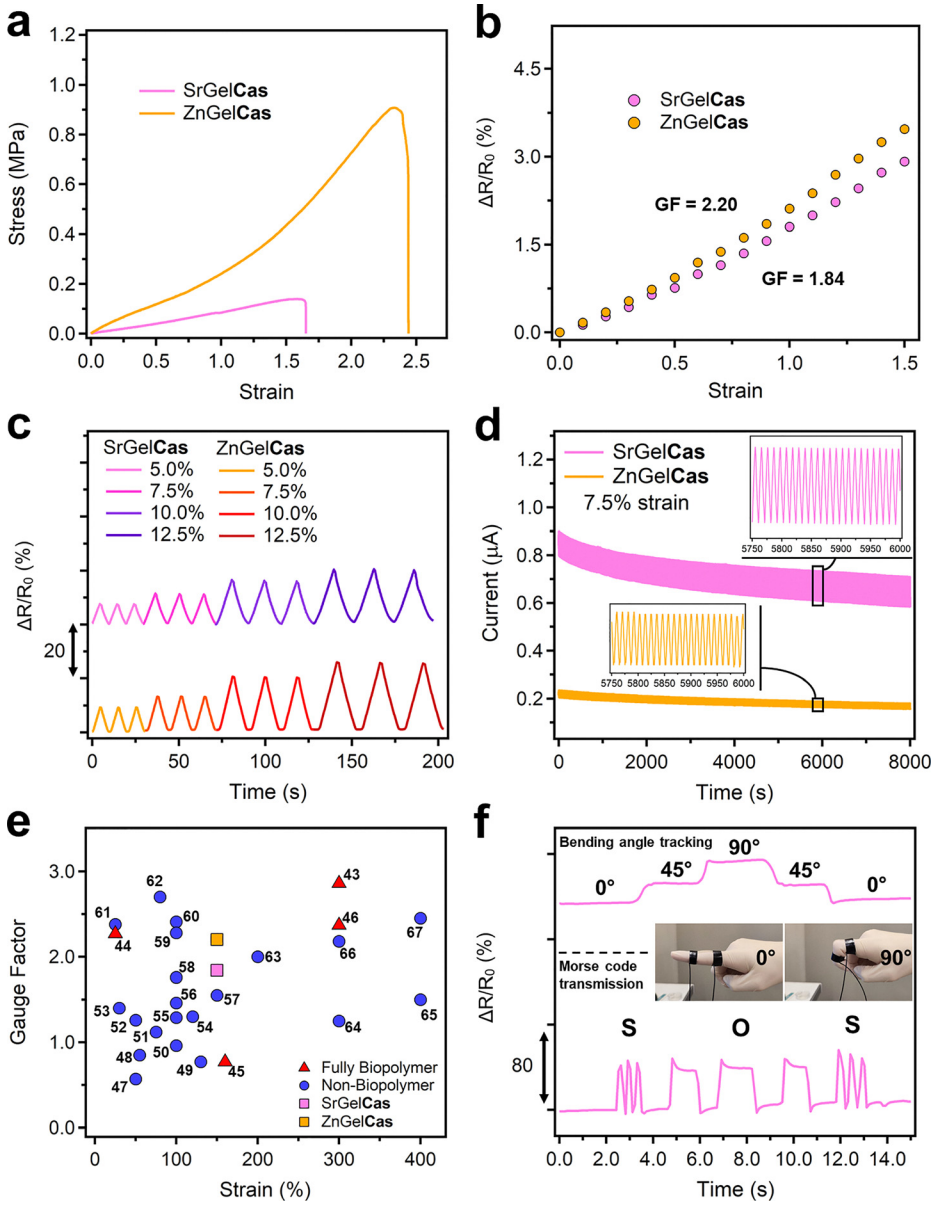

Fig. 5 (a) Tensile stress–strain curves of ZnGelCas and SrGelCas hydrogels, highlighting the strong ion-dependent modulation of stiffness. (b) Relative resistance variation ($\Delta R/R_0$) under tensile strain for SrGelCas and ZnGelCas, showing linear piezoresistive behavior with gauge factors (GF) of 1.84 and 2.20, respectively. (c) Stepwise strain-dependent $\Delta R/R_0$ response under cyclic tensile deformation at increasing strain amplitudes (5.0–12.5%), demonstrating reproducible and strain-amplitude-dependent electrical signals for both systems. The slowly varying baseline due to ionic current relaxation was subtracted for clarity. (d) Long-term cyclic response of SrGelCas and ZnGelCas under repeated deformation at fixed strain (7.5%); the 8000 s duration corresponds to approximately 800 deformation cycles. ZnGelCas exhibits a more stable signal amplitude over prolonged cycling, indicating enhanced mechanical and electrical robustness under repeated deformation, which is advantageous for more demanding sensing applications. (e) Benchmarking plot comparing the gauge factor and working strain range of MGelCas sensors (this work) with reported organohydrogel stretchable sensors. Reference entries 43–46 correspond to fully biopolymer-based scaffolds, whereas entries 47–67 represent synthetic or hybrid organohydrogels. ZnGelCas and SrGelCas occupy a competitive regime among sustainable materials. (f) Proof-of-concept real-time strain sensing using SrGelCas, including bending-angle tracking (0°–90°) and Morse code transmission ("SOS"), evidencing rapid, reversible, and high-contrast signal output during repeated deformation.

To evaluate this concept, we prepared hybrid caseinate–gelatin–glycerol organohydrogels (MGelCas) crosslinked with representative stiff (Zn^{2+}) and soft (Sr^{2+}) ions (see Section S1.3 for preparation details). Gelatin–glycerol organohydrogels have been recently established as effective platforms for soft electronic materials, combining high flexibility with enhanced stability against environmental fluctuations.[43] Here, the introduction of caseinate serves as a mechanical design lever, extending the strategy we previously established with alginate–gelatin organohydrogels, where biopolymer blending and ion coordination were used synergistically to modulate stiffness for functional flexible materials.[44] The resulting transparent MGelCas strips (Fig. S21) retain the ion-specific mechanical contrast observed in aqueous MCas systems and display well-defined tensile behavior suitable for repeated deformation. Consistent with their position in the packing hierarchy, ZnGelCas exhibits a markedly higher Young's modulus/ultimate tensile strength (UTS) and a lower extensibility than SrGelCas (Fig. 5a and Table S7), confirming that Zn^{2+}-driven network compaction persists even within the organohydrogel environment. This compaction also manifests as a pronounced difference in final sample thickness: ZnGelCas shrinks to $\sim$630 μm, whereas SrGelCas remains thicker ($\sim$930 μm), reflecting the higher packing density of the Zn-coordinated network (Table S7).

Under uniaxial traction, both materials exhibit linear, reversible resistance variations ($\Delta R/R_0$), reflecting strain-induced modulation of ionic pathways. ZnGelCas reaches a gauge factor (GF) of 2.20, whereas SrGelCas shows 1.84 (Fig. 5b). The higher sensitivity of the Zn-crosslinked network reflects its denser microstructure, where small geometric perturbations more strongly influence channel tortuosity and ion mobility. These results demonstrate that ionic coordination dictates both tensile stiffness and electromechanical transduction, establishing a practical route for tuning strain sensitivity in protein-based soft materials.

To assess signal reproducibility under dynamic operation, the piezoresistive response of MGelCas was examined under cyclic tensile deformation. Stepwise strain tests (5.0–12.5%) reveal stable, repeatable $\Delta R/R_0$ oscillations with amplitudes that increase systematically with strain for both SrGelCas and ZnGelCas (Fig. 5c), confirming reversible electromechanical transduction within the operational window. Long-term cycling at fixed strain (7.5%) demonstrates sustained signal modulation over $\sim$800 deformation cycles (8000 s), with ZnGelCas exhibiting a more stable response amplitude than SrGelCas (Fig. 5d). Extended cycling tests further confirm the high operational stability of ZnGelCas under prolonged deformation, highlighting its suitability for more demanding sensing conditions (Fig. S22). This behavior is consistent with the higher packing density and mechanical robustness of the Zn^{2+}-crosslinked network, underscoring the role of ion-directed compaction in enhancing durability under repeated deformation.

To contextualize performance, we compared MGelCas with reported biopolymer-based and synthetic hydrogel sensors (Fig. 5e). Both ZnGelCas and SrGelCas occupy a competitive region of the GF–strain landscape for organohydrogels and represent one of the few fully biopolymer-based scaffolds reported in this field.[43–67] At the same time, normalization of the gauge factor by the Young's modulus (GF/YM, Table S7) reveals a substantially higher effective electromechanical sensitivity for SrGelCas ($\approx$24.2 MPa^{-1}) than for ZnGelCas ($\approx$9.5 MPa^{-1}), highlighting the crucial role of network compliance in strain transduction. This positions caseinate (previously absent from soft-electronics research) as a highly tunable, sustainable platform for strain sensing. More broadly, the present results suggest that caseinate-based organohydrogels could also be extended in the future toward structured or printed soft-sensing platforms, as explored in other hydrogel-based systems.[68]

Finally, SrGelCas, representative of the softer and more compliant regime within the MGelCas platform, was integrated into a simple wearable-sensor configuration to demonstrate real-time operation under gentle mechanical inputs. Owing to its lower stiffness and higher deformability, SrGelCas accurately tracks bending angles from 0° to 90° with high signal fidelity and can encode temporal inputs such as Morse code sequences ("SOS"), yielding sharp and reproducible $\Delta R/R_0$ responses during operation (Fig. 5f). These results highlight how ion identity enables access to distinct operational regimes within the same material platform, with softer networks favoring low-demand, highly conformable wearable sensing, while denser networks are better suited for mechanically demanding applications. In light of our previous demonstration that analogous ionically crosslinked biopolymer organohydrogels respond to temperature and humidity, the present MGelCas systems are also promising candidates for multimodal sensing beyond strain.[44] Collectively, this versatility confirms MCas and MGelCas as programmable building blocks for soft, biocompatible sensing technologies.

Conclusions

This work introduces a previously unexplored class of ionically crosslinked hydrogels based on sodium caseinate, a renewable, amphiphilic protein widely available as a by-product of the food industry and endowed with a rich landscape of coordination-active functional groups. By leveraging its coordination properties towards multivalent metal cations, we demonstrate that high-concentration NaCas solutions can undergo rapid gelation, forming robust, freestanding hydrogels through non-covalent ionic crosslinking. A broad series of cations (Ca^{2+}, Sr^{2+}, Ba^{2+}, Mn^{2+}, Cu^{2+}, Zn^{2+}, Fe^{3+}, Al^{3+}, Zr^{4+}) was systematically investigated, revealing strong ion-specific modulation of the resulting hydrogels' physicochemical properties.

Comprehensive characterization using FTIR, XPS, SAXS, DSC, SEM, and mechanical testing revealed a direct link between ion identity, network density, and mechanical stiffness—culminating in an empirical operational packing scale that offers a foundational design tool for future caseinate-based materials.

Building on these insights, we translated the ion-programmed mechanical properties of MCas into functional soft-electronic behavior. Caseinate–gelatin–glycerol organohydrogels (MGelCas) formulated with representative soft (Sr^{2+}) and stiff (Zn^{2+}) crosslinkers were shown to operate as reproducible piezoresistive soft sensors, where tensile deformation generates stable, linear resistance variations. The two systems display gauge factors of 1.84 and 2.20 (SrGelCas and ZnGelCas), placing them toward the upper side of the typical performance range of state-of-the-art organohydrogel strain sensors, which generally span gauge factors of ~0.5–3. Their ability to detect bending angles and encode temporal input patterns further highlights their suitability for wearable and human–motion sensing.

All in all, this study positions ionically crosslinked caseinate hydrogels as a versatile and sustainable platform for programmable soft materials. By bridging protein chemistry with ionic coordination, we establish a general route to mechanically tunable, bio-derived hydrogels and organohydrogels, opening new opportunities in soft electronics, wearable sensing, and bioinspired materials design.

Author contributions

P. T., V. M. G., A. C., M. B. and P. S. conceived the experiments and designed the study. P. T. and V. L. prepared the samples and performed the physicochemical characterization. V. M. G. performed the XPS analysis. P. T., V. M. G., A. C., M. B. and P. S. discussed the results and contributed to the interpretation of data. P. T., V. M. G., A. C., M. B. and P. S. cowrote the paper. All authors have given approval to the final version of the manuscript.

Conflicts of interest

There are no conflicts to declare.

Data availability

All data supporting the findings of this study are available within the article and its supplementary information (SI). Supplementary information: detailed experimental procedures (Sections S1–S11), Fig. S1–S22 and Tables S1–S7. See DOI: https://doi.org/10.1039/d6mh00390g.

Acknowledgements

We are grateful to the financial supports from the CSGI (Consorzio Interuniversitario per lo Sviluppo dei Sistemi a Grande Interfase), the MUR-Italy (''Progetto Dipartimenti di Eccellenza 2023–2027'' and ''Progetto Dipartimenti di Eccellenza 2018–2022'' (58503DIP_ECC) allocated to Department of Chemistry ''Ugo Schiff''), the National Recovery and Resilience Plan (NRRP), Mission 4 Component 2 ''Dalla ricerca all'impresa'' —Call for tender no. 341 of 15/03/2022 of Italian Ministry of University and Research funded by the European Union – NextGenerationEU, CUP: B83C22004890007, the Agence Nationale de la Recherche through the Interdisciplinary Thematic Institute SysChem *via* the IdEx Unistra (ANR-10-IDEX-0002) within the program Investissement d'Avenir, the Foundation Jean-Marie Lehn, the Institut Universitaire de France (IUF). Prof. Mirko Severi is gratefully acknowledged for the ICP-AES measurements.

References

1 C. Wang, C. Wang, Z. Huang and S. Xu, *Adv. Mater.*, 2018, **30**(50), 1801368, DOI: 10.1002/adma.201801368.
2 H. Zhu, J. Wang, X. Yang, B. Zhang and Z. Wang, *Adv. Mater.*, 2025, **37**(22), 2413112, DOI: 10.1002/adma.202413112.
3 Y. Jeong, P. Tordi, A. Tamayo, B. Han, M. Bonini and P. Samorì, *Adv. Funct. Mater.*, 2025, **35**(50), e09607, DOI: 10.1002/adfm.202509607.
4 X. Dang, S. Han, J. Tang and X. Wang, *Aggregate*, 2025, **6**(10), e70121, DOI: 10.1002/agt2.70121.
5 C. Wang, T. Yokota and T. Someya, *Chem. Rev.*, 2021, **121**(4), 2109–2146, DOI: 10.1021/acs.chemrev.0c00897.
6 P. Tordi, F. Ridi, P. Samorì and M. Bonini, *Adv. Funct. Mater.*, 2025, **35**(9), 2416390, DOI: 10.1002/adfm.202416390.
7 D. Ji, J. M. Park, M. S. Oh, T. L. Nguyen, H. Shin, J. S. Kim, D. Kim, H. S. Park and J. Kim, *Nat. Commun.*, 2022, **13**(1), 3019, DOI: 10.1038/s41467-022-30691-z.
8 P. Tordi, V. Montes-García, A. Tamayo, M. Bonini, P. Samorì and A. Ciesielski, *Small*, 2025, **21**(33), 2503937, DOI: 10.1002/smll.202503937.
9 A. Joshi, S. Choudhury, V. S. Baghel, S. Ghosh, S. Gupta, D. Lahiri, G. K. Ananthasuresh and K. Chatterjee, *Adv. Healthcare Mater.*, 2023, **12**(24), 2300701, DOI: 10.1002/adhm.202300701.
10 Y. Shen, A. Levin, A. Kamada, Z. Toprakcioglu, M. Rodriguez-Garcia, Y. Xu and T. P. J. Knowles, *ACS Nano*, 2021, **15**(4), 5819–5837, DOI: 10.1021/acsnano.0c08510.
11 J. D. Brodin, X. I. Ambroggio, C. Tang, K. N. Parent, T. S. Baker and F. A. Tezcan, *Nat. Chem.*, 2012, **4**(5), 375–382, DOI: 10.1038/nchem.1290.
12 P. Ringler and G. E. Schulz, *Science*, 2003, **302**(5642), 106–109, DOI: 10.1126/science.1088074.
13 J. P. Schneider, D. J. Pochan, B. Ozbas, K. Rajagopal, L. Pakstis and J. Kretsinger, *J. Am. Chem. Soc.*, 2002, **124**(50), 15030–15037, DOI: 10.1021/ja027993g.
14 L. A. Haines, K. Rajagopal, B. Ozbas, D. A. Salick, D. J. Pochan and J. P. Schneider, *J. Am. Chem. Soc.*, 2005, **127**(48), 17025–17029, DOI: 10.1021/ja054719o.
15 L. E. R. O'Leary, J. A. Fallas, E. L. Bakota, M. K. Kang and J. D. Hartgerink, *Nat. Chem.*, 2011, **3**(10), 821–828, DOI: 10.1038/nchem.1123.
16 Y. Zhou, R. Chang, Z. Yang, Q. Guo, M. Wang, B. Jia, B. Li, B. Deng, Y. Ren, H. Zhu, X. Wang, Q. Wang, H. Wen, H. Zhang, J. Yu, Y. Chen and K. Liu, *J. Am. Chem. Soc.*, 2025, **147**(3), 2335–2349, DOI: 10.1021/jacs.4c10882.

17 Y. Lu, Y. Chen, Y. Zhu, J. Zhao, K. Ren, Z. Lu, J. Li and Z. Hao, *Polymers*, 2023, **15**(24), 4652, DOI: 10.3390/polym15244652.
18 C. G. de Kruif, T. Huppertz, V. S. Urban and A. V. Petukhov, *Adv. Colloid Interface Sci.*, 2012, **171–172**, 36–52, DOI: 10.1016/j.cis.2012.01.002.
19 H. E. Swaisgood, *J. Dairy Sci.*, 1993, **76**(10), 3054–3061, DOI: 10.3168/jds.S0022-0302(93)77645-6.
20 E. Dickinson and E. Davies, *Colloids Surf., B*, 1999, **12**(3), 203–212, DOI: 10.1016/S0927-7765(98)00075-7.
21 B. G. Shilpashree, S. Arora, P. Chawla and V. Sharma, *LWT*, 2022, **157**, 113116, DOI: 10.1016/j.lwt.2022.113116.
22 M. Sugiarto, A. Ye and H. Singh, *Food Chem.*, 2009, **114**(3), 1007–1013, DOI: 10.1016/j.foodchem.2008.10.062.
23 C. Schorsch, H. Carrie, A. H. Clark and I. T. Norton, *Int. Dairy J.*, 2000, **10**(8), 519–528, DOI: 10.1016/S0958-6946(00)00052-2.
24 P. Chr. Lorenzen, E. Schlimme and N. Roos, *Food Nahr.*, 1998, **42**(03–04), 151–154, DOI: 10.1002/(SICI)1521-3803(199808)42:03/04<151:AID-FOOD151>3.0.CO;2-E.
25 M. Philippe, Y. Le Graët and F. Gaucheron, *Food Chem.*, 2005, **90**(4), 673–683, DOI: 10.1016/j.foodchem.2004.06.001.
26 P. Pomastowski, M. Sprynskyy and B. Buszewski, *Colloids Surf., B*, 2014, **120**, 21–27, DOI: 10.1016/j.colsurfb.2014.03.009.
27 T. G. Parker and D. G. Dalgleish, *J. Dairy Res.*, 1981, **48**(1), 71–76, DOI: 10.1017/S0022029900021476.
28 M. Xiao, J. Meng, H. Zhang, Z. Wu and Z. Li, *Adv. Mater.*, 2025, **37**(40), e06436, DOI: 10.1002/adma.202506436.
29 S. Qin, Y. Niu, Y. Zhang, W. Wang, J. Zhou, Y. Bai and G. Ma, *Biomacromolecules*, 2024, **25**(6), 3217–3248, DOI: 10.1021/acs.biomac.3c01072.
30 J. L. Bideau, L. Viau and A. Vioux, *Chem. Soc. Rev.*, 2011, **40**(2), 907–925, DOI: 10.1039/C0CS00059K.
31 T. P. Lodge and T. Ueki, *Acc. Chem. Res.*, 2016, **49**(10), 2107–2114, DOI: 10.1021/acs.accounts.6b00308.
32 G. O. Lloyd and J. W. Steed, *Nat. Chem.*, 2009, **1**(6), 437–442, DOI: 10.1038/nchem.283.
33 W. Zhao, Y. Zheng, M. Jiang, T. Sun, A. Huang, L. Wang, W. Jiang and Q. Zhang, *Sci. Adv.*, 2023, **9**(43), eadk2098, DOI: 10.1126/sciadv.adk2098.
34 L. G. L. Nascimento, F. Casanova, N. F. Noguera Silva, A. V. N. Teixeira and A. Fernandes de Carvalho, *Food Chem.*, 2020, **314**, 126063, DOI: 10.1016/j.foodchem.2019.126063.
35 P. Tordi, R. Gelli, S. Tamantini and M. Bonini, *Int. J. Biol. Macromol.*, 2025, **306**, 141196, DOI: 10.1016/j.ijbiomac.2025.141196.
36 P. Tordi, R. Gelli, F. Ridi and M. Bonini, *Carbohydr. Polym.*, 2024, **326**, 121586, DOI: 10.1529/biophysj.106.083691.
37 B. Hammouda and D. Worcester, *Biophys. J.*, 2006, **91**(6), 2237–2242, DOI: 10.1529/biophysj.106.083691.
38 R. A. Hule, R. P. Nagarkar, A. Altunbas, H. R. Ramay, M. C. Branco, J. P. Schneider and D. J. Pochan, *Faraday Discuss.*, 2008, **139**(0), 251–264, DOI: 10.1039/B717616C.
39 G. Ochbaum and R. Bitton, *Self-assembling Biomaterials*, Woodhead Publishing, 2018, pp. 291–304, DOI: 10.1016/B978-0-08-102015-9.00015-0.
40 E. M. Saffer, M. A. Lackey, D. M. Griffin, S. Kishore, G. N. Tew and S. R. Bhatia, *Soft Matter*, 2014, **10**(12), 1905–1916, DOI: 10.1039/C3SM52395K.
41 D. Katrantzi, S. Micklethwaite, N. Hondow, A. Brown and L. Dougan, *Faraday Discuss.*, 2025, **260**(0), 55–81, DOI: 10.1039/D4FD00204K.
42 D. McDowall, D. J. Adams and A. M. Seddon, *Soft Matter*, 2022, **18**(8), 1577–1590, DOI: 10.1039/D1SM01707A.
43 P. Tordi, A. Tamayo, Y. Jeong, B. Han, T. Al Kayal, A. Cavallo, M. Bonini and P. Samorì, *Adv. Funct. Mater.*, 2026, **36**(23), e20762, DOI: 10.1002/adfm.202520762.
44 P. Tordi, A. Tamayo, Y. Jeong, M. Bonini and P. Samorì, *Adv. Funct. Mater.*, 2024, **34**(52), 2410663, DOI: 10.1002/adfm.202410663.
45 W. Zhang, C. Ma, L. Huang, W. Guo, D. Li, J. Bian and M. Ma, *Macromol. Mater. Eng.*, 2021, **306**(12), 2100549, DOI: 10.1002/mame.202100549.
46 M. Bian, G. Hou, Z. Tan, L. Zhang, S. Miao, B. Zheng and F. Zhou, *Carbohydr. Polym.*, 2025, **352**, 123200, DOI: 10.1016/j.carbpol.2024.123200.
47 L. Ye, R. Yang, X. Yu, X. Sun and H. Liang, *Soft Matter*, 2024, **20**(7), 1573–1582, DOI: 10.1039/d3sm01281f.
48 G. Mogli, I. Roppolo, A. Chiappone and S. Stassi, *Appl. Mater. Today*, 2025, **44**, 102675, DOI: 10.1016/j.apmt.2025.102675.
49 X. Liu, L. Du, Y. Ma, T. Li, S. Chen, J. Yang, Z. Ran, L. Zhou, Q. Dong, W. Zheng and Z. Jiang, *Int. J. Biol. Macromol.*, 2024, **279**, 135029, DOI: 10.1016/j.ijbiomac.2024.135029.
50 M. Li, D. Chen, X. Sun, Z. Xu, Y. Yang, Y. Song and F. Jiang, *Carbohydr. Polym.*, 2022, **284**, 119199, DOI: 10.1016/j.carbpol.2022.119199.
51 Y. Yang, B. Song, J. Zhang, N. Dan and H. Gu, *Biomacromolecules*, 2024, **25**(8), 5359–5373, DOI: 10.1021/acs.biomac.4c00803.
52 L. Xu, X. Li, J. Gao, M. Yan and Q. Wang, *Mater. Today Commun.*, 2024, **40**, 109542, DOI: 10.1016/j.mtcomm.2024.109542.
53 Y. Cheng, X. Ren, G. Gao and L. Duan, *Carbohydr. Polym.*, 2019, **223**, 115051, DOI: 10.1016/j.carbpol.2019.115051.
54 J. Lyu, Q. Zhou, H. Wang, Q. Xiao, Z. Qiang, X. Li, J. Wen, C. Ye and M. Zhu, *Adv. Sci.*, 2023, **10**(9), 2206591, DOI: 10.1002/advs.202206591.
55 D. Bi, N. Qu, W. Sheng, T. Lin, S. Huang, L. Wang and R. Li, *ACS Appl. Mater. Interfaces*, 2024, **16**(9), 11914–11929, DOI: 10.1021/acsami.3c18631.
56 Z. Li, P. Liu, S. Chen, B. Wang, S. Liu, E. Cui, F. Li, Y. Yu, W. Pan, N. Tang and Y. Gu, *Int. J. Biol. Macromol.*, 2024, **258**, 129054, DOI: 10.1016/j.ijbiomac.2023.129054.
57 L. Zhang, O. Hu, J. Zhang, L. Hou, D. Ye, X. Jiang and G. Xiao, *Cellulose*, 2022, **29**(17), 9323–9339, DOI: 10.1007/s10570-022-04844-8.
58 L. He, J. Wang, S. Weng and X. Jiang, *Carbohydr. Polym.*, 2023, **306**, 120587, DOI: 10.1016/j.carbpol.2023.120587.
59 Z. Guo, H. Zhang, W. Xie, A. Tang and W. Liu, *Addit. Manuf.*, 2023, **77**, 103824, DOI: 10.1016/j.addma.2023.103824.
60 Q. Yu, Z. Qin, F. Ji, S. Chen, S. Luo, M. Yao, X. Wu, W. Liu, X. Sun, H. Zhang, Y. Zhao, F. Yao and J. Li, *Chem. Eng. J.*, 2021, **404**, 126559, DOI: 10.1016/j.cej.2020.126559.

61 R. Zhao, J. Luo, J. Liu, T. Ke, J. Zhang, C. Gaidau, J. Zhou and H. Gu, *Chem. Mater.*, 2024, **36**(17), 8141–8158, DOI: 10.1021/acs.chemmater.4c00504.
62 H. Liu, Z. Chen, X. Lin, X. Zhang, Y. Cai, Y. Zhang, B. Sun, X. Mei, W. Lyu, R. B. Kaner, M. Zhu and Y. Liao, *Chem. Mater.*, 2024, **36**(12), 6100–6113, DOI: 10.1021/acs.chemmater.4c00846.
63 B. Song, X. Dai, X. Fan and H. Gu, *J. Mater. Sci. Technol.*, 2024, **181**, 91–103, DOI: 10.1016/j.jmst.2023.10.008.
64 J. J. Paik, B. Jang, S. Nam and L. J. Guo, *Adv. Healthcare Mater.*, 2023, **12**(22), 2300076, DOI: 10.1002/adhm.202300076.
65 H. Sun, Y. Han, M. Huang, J. Li, Z. Bian, Y. Wang, H. Liu, C. Liu and C. Shen, *Chem. Eng. J.*, 2024, **480**, 148305, DOI: 10.1016/j.cej.2023.148305.
66 E. Feng, J. Li, G. Zheng, Z. Yan, X. Li, W. Gao, X. Ma and Z. Yang, *ACS Sustainable Chem. Eng.*, 2021, **9**(21), 7267–7276, DOI: 10.1021/acssuschemeng.1c01209.
67 N. Qu, W. Zhou, T. Lin, S. Qin, P. Ma and S. Huang, *Colloids Surf. Physicochem. Eng. Asp.*, 2025, **717**, 136778, DOI: 10.1016/j.colsurfa.2025.136778.
68 A. Joshi, S. Choudhury, A. Majhi, S. Parasuram, V. S. Singh Baghel, S. Chauhan, S. Khanra, D. Lahiri and K. Chatterjee, *Biomater. Sci.*, 2025, **13**(17), 4706–4716, DOI: 10.1039/D5BM00166H.